MRS Advances

Epitaxial Growth and Bandgap Control of $Ni_{1-x}Mg_xO$ Thin Film Grown by Mist Chemical Vapor Deposition Method

Takumi Ikenoue[1], Satoshi Yoneya[1], Masao Miyake[1], and Tetsuji Hirato[1]

[1]*Graduate School of Energy Science, Kyoto University, Kyoto 606-8501, Japan*

ABSTRACT

Wide-bandgap oxide semiconductors have received significant attention as they can produce devices with high output and breakdown voltage. p-Type conductivity control is essential to realize bipolar devices. Therefore, as a rare wide-bandgap p-type oxide semiconductor, NiO (3.7 eV) has garnered considerable attention. In view of the heterojunction device with Ga_2O_3 (4.5–5.0 eV), a p-type material with a large bandgap is desired. Herein, we report the growth of a $Ni_{1-x}Mg_xO$ thin film, which has a larger bandgap than NiO, on α-Al_2O_3 (0001) substrates that was developed using the mist chemical vapor deposition method. The $Ni_{1-x}Mg_xO$ thin films epitaxially grown on α-Al_2O_3 substrates showed crystallographic orientation relationships identical to those of NiO thin films. The Mg composition of $Ni_{1-x}Mg_xO$ was easily controlled by the Mg concentration of the precursor solution. The $Ni_{1-x}Mg_xO$ thin film with a higher Mg composition had a larger bandgap, and the bandgap reached 3.9 eV with a $Ni_{1-x}Mg_xO$ thin film with $x = 0.28$. In contrast to an undoped $Ni_{1-x}Mg_xO$ thin film showing insulating properties, the Li-doped $Ni_{1-x}Mg_xO$ thin film had resistivities of 10^1–10^5 Ω·cm depending on the Li precursor concentration, suggesting that Li effectively acts as an acceptor.

INTRODUCTION

Wide-bandgap semiconductors have attracted wide attention owing to their ability of realizing high output and high breakdown voltage power devices. The bandgaps of wide-bandgap semiconductors such as GaN (3.4 eV) and Ga_2O_3 (4.5–5.0 eV) have been further expanded using alloy crystals with AlN (6.3 eV) and Al_2O_3 (8.8 eV), respectively. Oxide semiconductors typified by Ga_2O_3 have been studied as they can obtain films under atmospheric pressure and can be expected to further increase the bandgap that directly affects device performance[1]. Although the demand for wide-bandgap oxide semiconductors is increasing, many wide-bandgap oxide semiconductors, including Ga_2O_3,

exhibit only n-type conductivity. Therefore, as it is a rare wide-bandgap p-type oxide semiconductor, NiO (3.7 eV) has attracted increasing attention. In view of the fabrication of heterojunction devices with materials such as Ga_2O_3, the bandgap of NiO is slightly small (3.7 eV), and a p-type oxide semiconductor with a larger bandgap is required. Therefore, we focused on $Ni_{1-x}Mg_xO$, which is a semiconductor alloy crystal comprising NiO and MgO. Both NiO and MgO crystallize in the cubic rock-salt structure, and $Ni_{1-x}Mg_xO$ is stable over the entire composition range with no phase transition or significant changes in lattice parameters, with a structural mismatch of only 0.8% at maximum[2]. Therefore, potentially, the bandgap can be expanded while maintaining p-type conduction from 3.7 eV for NiO to 7.8 eV[3] for MgO. With regard to $Ni_{1-x}Mg_xO$, several studies have been conducted on epitaxial growth via vacuum processes such as molecular beam epitaxy[4] and pulsed laser deposition[5]; however, growth via the solution atmospheric pressure process is limited to polycrystalline films[6], and there have only been few studies on epitaxial growth. In previous studies, we reported the epitaxial growth of NiO thin films on α-Al_2O_3 substrates via mist chemical vapor deposition (CVD)[7]. By this method, high-quality oxide thin films can be grown at atmospheric pressure and semiconductor alloy crystals such as $Mg_xZn_{1-x}O$[8,9] and $(Al_xGa_{1-x})_2O_3$[10] can be easily obtained by mixing precursor source solutions.

Herein, we report the increase in bandgap due to the alloy crystals of NiO with MgO via mist CVD by controlling the Ni and Mg concentration in the precursor solution. The Mg composition in the $Ni_{1-x}Mg_xO$ film, i.e., the bandgap of the $Ni_{1-x}Mg_xO$ thin film, was easily controlled by the Mg concentration of the precursor solution via mist CVD. In addition, the conductivity of $Ni_{1-x}Mg_xO$ thin films was found to be controlled via Li-doping.

EXPERIMENTAL DETAILS

Growth of $Ni_{1-x}Mg_xO$ thin film

Prior to the growth of $Ni_{1-x}Mg_xO$, the α-Al_2O_3 (0001) substrates were annealed in air at 1050 °C for 4 h to obtain an atomically flat surface and then sequentially cleaned in acetone, methanol, and deionized water using an ultrasonic cleaner. Undoped and Li-doped $Ni_{1-x}Mg_xO$ thin films were grown via mist CVD; this procedure is described in detail in previous studies[1,7,8,11–13]. The growth conditions are summarized in Table I. In a previous study, nickel acetylacetonate ($Ni(acac)_2$) was used as a precursor for NiO thin films[7]. Similarly, the precursors used for the undoped $Ni_{1-x}Mg_xO$ thin-film growth was $Ni(acac)_2$ and magnesium acetylacetonate ($Mg(acac)_2$), which were diluted in deionized water at a total concentration of 0.020 mol/L. The Mg concentration in a source solution is determined from the ratio of the concentration of $Mg(acac)_2$ to the concentration of $Mg(acac)_2$ and $Ni(acac)_2$ (Mg/(Ni+Mg)) and is expressed in at.%. Following this, ethylenediamine (EDA) was added, which is a complex-forming additive. For Li-doped $Ni_{1-x}Mg_xO$ thin films, the precursor solution was obtained by adding lithium acetylacetonate (Li(acac)) to the aqueous precursor solution containing 0.04 mol/L $Ni(acac)_2$ and 0.16 mol/L $Mg(acac)_2$. The Li concentration was varied from 0 to 2 mmol/L such that the Li concentration was 0–10 mol.% with respect to Ni plus Mg. Dry air was used for the carrier gas and dilution gases, with flow rates of 4.0 and 2.0 L/min, respectively.

Table I. Growth conditions of $Ni_{1-x}Mg_xO$ thin films.

Ni source, concentration	$Ni(acac)_2$, 0–0.020 mol/L	Total concentration
Mg source, concentration	$Mg(acac)_2$, 0–0.020 mol/L	0.020 mol/L
Complex agent, concentration	EDA, 0.040 mol/L	
Dopant, concentration	Li(acac), 0–0.002 mol/L	
Solvent	Deionized water	
Carrier gas, flow rate	Dry air, 4 L/min	
Dilution gas, flow rate	Dry air, 2 L/min	
Growth temperature	700 °C	
Growth time	10 min	
Substrate, size	α-Al_2O_3 (0001), 10 × 10 mm	

Characterizations

To evaluate crystal structure, X-ray diffraction (XRD) analysis was performed using a Panalytical X'pert PRO MPD system. The composition of the films was determined via energy dispersive spectroscopy (EDS; INCAx-act, Oxford Instruments) and X-ray photoelectron spectroscopy (XPS; JPS-9030, JEOL). The surface morphology of the films was observed via atomic force microscopy (AFM) (SII Nano Technology, Nano Navi IIs Nanocute). UV–Vis spectral analysis was performed using a UV–Vis spectrophotometer (Shimadzu, UV-2450). The electrical resistivity of the films was determined via the four terminal method using a source measure unit (Keithley, 2450 SourceMeter); the film thickness was obtained from X-ray reflectivity measurements.

RESULTS AND DISCUSSION

Figure 1 shows the XRD patterns from the 2θ/θ scan of $Ni_{1-x}Mg_xO$ thin films obtained from each Mg concentration precursor solution. Under all precursor solutions, diffraction peaks of $Ni_{1-x}Mg_xO$ (111) and (222) were observed in addition to the diffraction peak of the α-Al_2O_3 (0006) substrate. Figures 1 (b) and (c) show expanded $Ni_{1-x}Mg_xO$ (111) and (222) diffraction peaks. Under the precursor solution containing a Mg concentration of 50% or less, Laue fringes were observed, suggesting that the $Ni_{1-x}Mg_xO$ thin film was of high quality. As the Mg concentration in the precursor solution increased, the diffraction peak of $Ni_{1-x}Mg_xO$ (111) and (222) shifted from the diffraction position of bulk NiO to that of bulk MgO. This result suggests that the Mg composition in the $Ni_{1-x}Mg_xO$ thin film can be controlled by the Mg concentration of the precursor solution. Figure 2 shows a pole figure of the $Ni_{1-x}Mg_xO$ thin film obtained from the source solution with a Mg concentration of 50%. Similar pole figures were observed for all $Ni_{1-x}Mg_xO$ thin films obtained from all Mg concentrations. Based on the XRD and X-ray pole figure measurements, the epitaxial relationships between $Ni_{1-x}Mg_xO$ and α-Al_2O_3 can be written as $Ni_{1-x}Mg_xO(111)[\bar{1}10]\|\alpha\text{-}Al_2O_3(0001)[01\bar{1}0]$ and $Ni_{1-x}Mg_xO$ $(111)[1\bar{1}0]\|\alpha\text{-}Al_2O_3(0001)[01\bar{1}0]$, similar to that described in a previous study on NiO[7].

Figure 3 shows the dependence of the Mg composition of the $Ni_{1-x}Mg_xO$ thin film on the Mg concentration in the precursor solution. Both compositions are expressed in at.% and calculated as Mg/(Mg+Ni). As suggested by the XRD analysis, the Mg composition in the $Ni_{1-x}Mg_xO$ film monotonously increases as the Mg concentration of the precursor solution increases. The Mg composition in the $Ni_{1-x}Mg_xO$ thin film can be easily controlled by controlling the Mg and Ni concentration of the precursor solution. Even when the Mg concentration in the precursor solution reached 90%, the Mg composition in the $Ni_{1-x}Mg_xO$

thin film remained below 30%. Because the growth conditions were optimized with NiO, the reaction efficiency of the Mg precursor and the uptake efficiency of Mg may be low. Re-examining the growth conditions may generate a $Ni_{1-x}Mg_xO$ thin film with higher Mg composition.

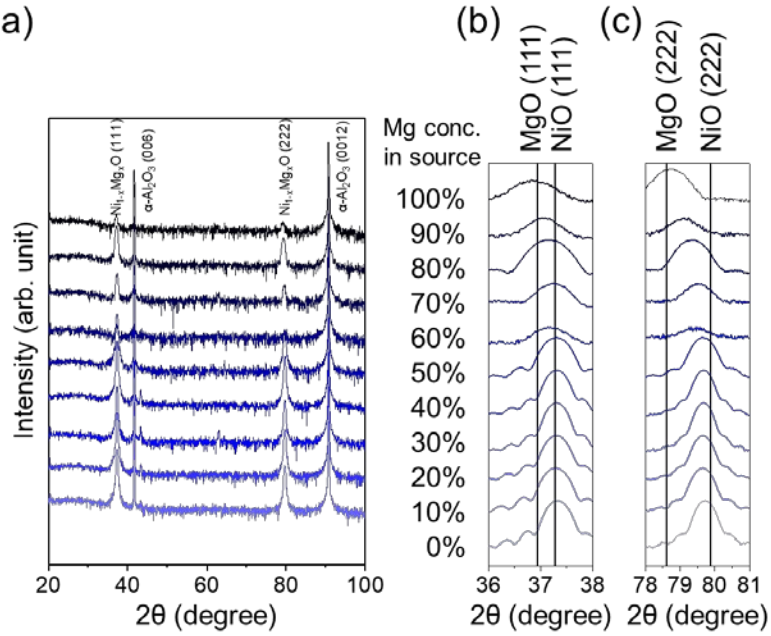

Figure 1. (a) X-ray diffraction patterns from the 2θ/θ scan of the $Ni_{1-x}Mg_xO$ thin films obtained from each Mg concentration precursor solution. Expanded views of the (b) $Ni_{1-x}Mg_xO$ (111) and (c) (222) diffraction peaks.

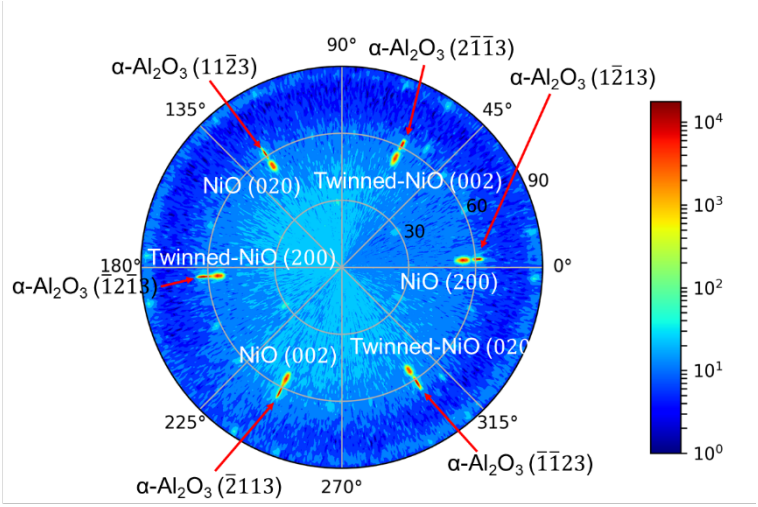

Figure 2. XRD pole figure for {002} planes of the $Ni_{1-x}Mg_xO$ thin film measured at 2θ = 43.383°. Diffraction of α-Al_2O_3 {11$\bar{2}$3} plane (2θ = 43.340°) is also observed in this pole figure.

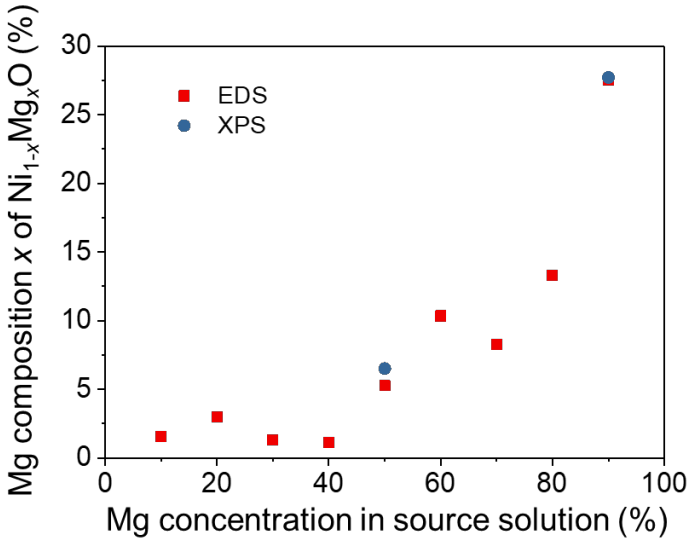

Figure 3. Dependence of the Mg composition of the $Ni_{1-x}Mg_xO$ thin film on the Mg concentration in the precursor solution.

The surface morphology of the $Ni_{1-x}Mg_xO$ thin film was investigated using AFM. The typical AFM image of the $Ni_{1-x}Mg_xO$ thin film obtained from the source solution with a Mg concentration of 50% (Fig. 4) shows that the film is composed of crystal grains in the range of 100–300 nm, which are derived from the domain structure.

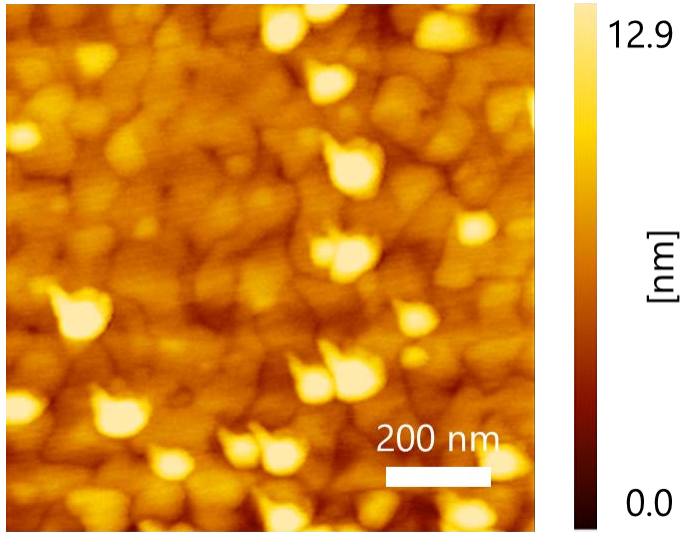

Figure 4. AFM image of $Ni_{1-x}Mg_xO$ thin film obtained from source solution with a Mg concentration of 50%.

Figure 5 shows the transmittance spectra and Tauc plot of the $Ni_{1-x}Mg_xO$ thin films with various Mg compositions. In the transmittance spectra, a marked decrease in the transmission rate occurred at wavelengths ranging from 350 to 300 nm depending on Mg composition, which is clearly due to absorption by $Ni_{1-x}Mg_xO$. The bandgaps calculated from the Tauc plot [$(\alpha h\nu)^2$–$h\nu$] also increased from 3.5 eV to 3.9 eV depending on the Mg composition. Figure 4 shows the composition dependence of the $Ni_{1-x}Mg_xO$ thin film bandgap as calculated from the Tauc plot in this work (large red square). The bandgaps of $Ni_{1-x}Mg_xO$ thin films in previous reports grown by the various methods[4,6,14–16] are also shown for comparison. The bandgaps observed herein have the same tendency as those of previous studies[17]: the bandgap increases with increasing Mg composition. The bandgap reached 3.9 eV with a $Ni_{1-x}Mg_xO$ thin film with x = 0.28.

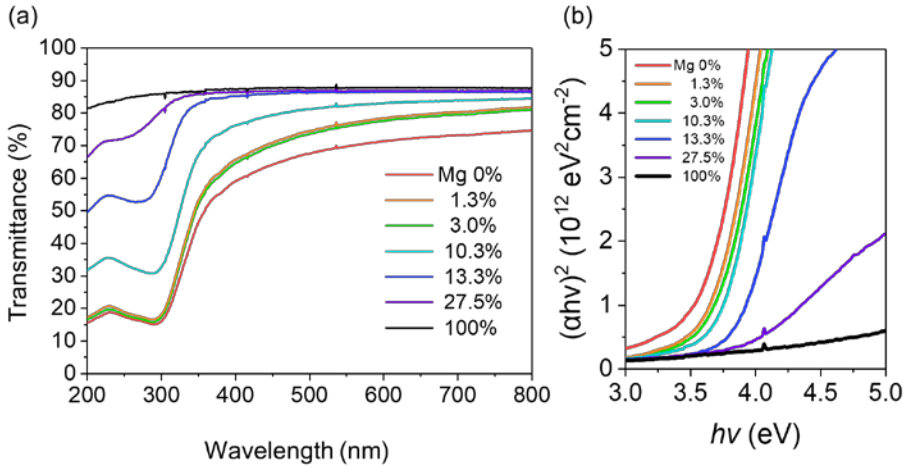

Figure 5. (a) Transmittance spectra and (b) Tauc plot of the $Ni_{1-x}Mg_xO$ thin films.

Finally, conductivity control via Li-doping was investigated. For Li-doping, a precursor solution having a Mg concentration of 80% and a Ni concentration of 20% was used. The $Ni_{1-x}Mg_xO$ thin film obtained using this precursor solution has a Mg composition of 13.3% and a bandgap of 3.8 eV. The same crystal structure, epitaxial orientation relationship, and optical properties as the undoped $Ni_{1-x}Mg_xO$ thin film as described above were obtained for the Li-doped $Ni_{1-x}Mg_xO$ thin films. Figure 6 shows the dependence of the Li-doped $Ni_{1-x}Mg_xO$ thin film resistivity on Li concentration. As the Li concentration in the precursor solution increased, the resistivity value of the Li-doped $Ni_{1-x}Mg_xO$ thin film decreased. Furthermore, they exhibited positive Seebeck coefficients, indicating their p-type conductivity. When the Li concentration was 10%, the resistivity was 43 Ωcm. This variation in resistivity demonstrates the same tendency as that of Li-doping in the NiO thin film on α-Al_2O_3[7], suggesting that both the increase in bandgap and p-type conductivity control were realized.

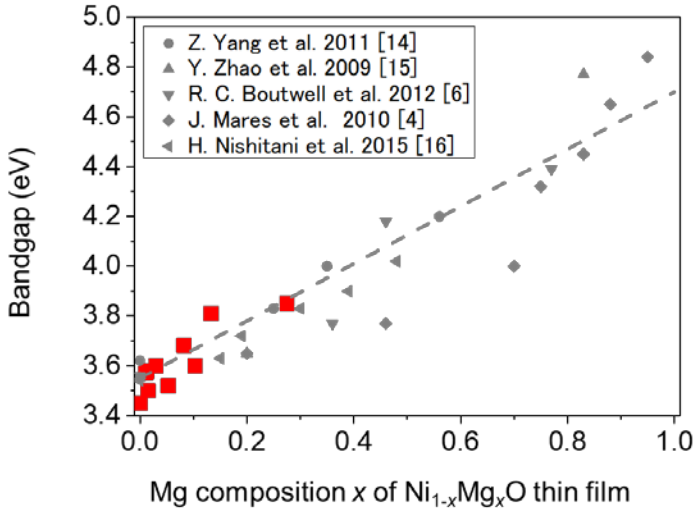

Figure 6. Dependence of the bandgap of the $Ni_{1-x}Mg_xO$ thin film on Mg composition.

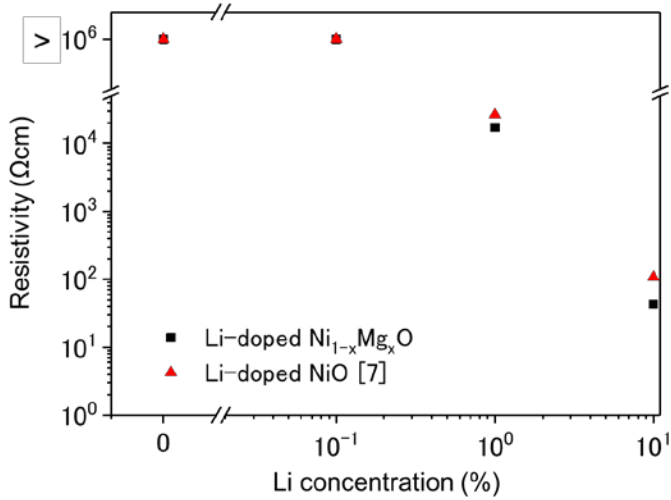

Figure 7. Dependence of the Li concentration on the resistivity of the Li-doped $Ni_{1-x}Mg_xO$ thin film.

CONCLUSIONS

In this study, $Ni_{1-x}Mg_xO$ thin films were epitaxially grown on α-Al_2O_3 substrates via mist CVD. The bandgap of $Ni_{1-x}Mg_xO$ thin films increased depending on the Mg composition in the $Ni_{1-x}Mg_xO$ thin film, which can be controlled by the Mg concentration in the precursor solution. The electrical resistivity of the $Ni_{1-x}Mg_xO$ thin film, which was higher than 10^6 Ωcm in the undoped sample, was improved to 10^1–10^5 Ωcm via Li-doping, indicating that Li can be effectively doped into $Ni_{1-x}Mg_xO$ thin films.

ACKNOWLEDGMENTS

This study was supported by Japan Society for Promotion of Science Early-Career Scientists (grant No. JP18K13788) and Grant-in-Aid for Scientific Research (C) (grant No. 20K04580).

References:

[1] D. Shinohara and S. Fujita, *Jpn. J. Appl. Phys.* **47**, 7311-7313 (2008). doi:10.1143/JJAP.47.7311.

[2] A. Kuzmin and N. Mironova, *J. Phys. Condens. Matter.* **10**, 7937-7944 (1998). doi:10.1088/0953-8984/10/36/004.

[3] D.M. Roessler and W.C. Walker, *Phys. Rev.* **159**, 733-738 (1967). doi:10.1103/PhysRev.159.733.

[4] J.W. Mares, C.R. Boutwell, A. Scheurer, M. Falanga and W. V. Schoenfeld, *Proc. SPIE* **7603**, 76031B (2010). doi:10.1117/12.841327.

[5] Y.M. Guo, L.P. Zhu, J. Jiang, L. Hu, C.L. Ye and Z.Z. Ye, *Appl. Phys. Lett.* **101**, 052109 (2012). doi:10.1063/1.4742172.

[6] R.C. Boutwell, M. Wei, A. Scheurer, J.W. Mares and W.V. Schoenfeld, *Thin Solid Films* **520**, 4302-4304 (2012). doi:10.1016/j.tsf.2012.02.065.

[7] T. Ikenoue, J. Inoue, M. Miyake and T. Hirato, *J. Cryst. Growth.* **507**, 379-383 (2019). doi:10.1016/j.jcrysgro.2018.11.032.

[8] H. Nishinaka, Y. Kamada, N. Kameyama and S. Fujita, *Phys. Status Solidi.* **247**, 1460-1463 (2010). doi:10.1002/pssb.200983247.

[9] K. Kaneko, T. Onuma, K. Tsumura, T. Uchida, R. Jinno, T. Yamaguchi, T. Honda and S. Fujita, *Appl. Phys. Express* **9**, 111102 (2016). doi:10.7567/APEX.9.111102.

[10] H. Ito, K. Kaneko and S. Fujita, *Jpn. J. Appl. Phys.* **51**, 100207 (2012). doi:10.1143/JJAP.51.100207.

[11] H. Nishinaka, Y. Kamada, N. Kameyama and S. Fujita, *Jpn. J. Appl. Phys.* **48**, 121103 (2009). doi:10.1143/JJAP.48.121103.

[12] K. Akaiwa and S. Fujita, *Jpn. J. Appl. Phys.* **51**, 070203 (2012). doi:10.1143/JJAP.51.070203.

[13] N. Suzuki, K. Kaneko and S. Fujita, *J. Cryst. Growth.* **364**, 30-33 (2013). doi:10.1016/j.jcrysgro.2012.11.065.

[14] Z.-G. Yang, L.-P. Zhu, Y.-M. Guo, Z.-Z. Ye and B.-H. Zhao, *Thin Solid Films* **519**, 5174-5177 (2011). doi:10.1016/j.tsf.2011.01.082.

[15] Y. Zhao, J. Zhang, D. Jiang, C. Shan, Z. Zhang, B. Yao, D. Zhao and D. Shen, *J. Phys. D. Appl. Phys.* **42**, 092007 (2009). doi:10.1088/0022-3727/42/9/092007.

[16] H. Nishitani, K. Ohta, S. Kitano, R. Hamano, M. Inada, T. Shimizu, S. Shingubara, H. Kozuka and T. Saitoh, *Appl. Phys. Express* **9**, 039201 (2016). doi:10.7567/APEX.9.039201.

[17] C.A. Niedermeier, M. Råsander, S. Rhode, V. Kachkanov, B. Zou, N. Alford and M.A. Moram, *Sci. Rep.* **6**, 31230 (2016). doi:10.1038/srep31230.